Hindawi
International Journal of Aerospace Engineering
Volume 2023, Article ID 9994093, 15 pages
https://doi.org/10.1155/2023/9994093

Research Article

Closed-Loop Fault Diagnosis of SDR Using Gap Metric, PCA, and Kalman's Principle

Hongfu Wang,[1] **Qinghua Zeng**,[1] **An Wang**,[2] **Zongyu Zhang**,[1] **and Weide Liu**[1]

[1]*College of Aeronautics and Astronautics, Sun Yat-sen University, Shenzhen, Guangdong Province 518107, China*
[2]*Institute of Air and Space Technology, China Aerodynamic Research and Development Center, Mianyang, Sichuan Province 621000, China*

Correspondence should be addressed to Qinghua Zeng; zqinghua@sysu.edu.cn

Received 22 February 2022; Revised 17 August 2022; Accepted 22 December 2022; Published 5 January 2023

Academic Editor: Jun-Wei Li

The measurement of the pressure in the gas generator (GG) plays a decisive role in the closed-loop regulation of the gas flow in a solid ducted rocket ramjet (SDR). Therefore, the fault detection and isolation (FDI) of the pressure sensors is particularly significant. Especially in the GG with double pressure feedback, there are issues such as less available data and sensor fault transmission, which make the FDI more difficult. In this paper, for the GG with double pressure feedback, firstly, the "Consistency Index" was constructed based on the principal component analysis (PCA) algorithm, which made it easier to evaluate the consistency of the measured values. Secondly, based on Kalman's principle, the redundancy information of the system was used to estimate the pressure in the GG. Finally, the gap metric between the measured pressure and the estimated pressure was employed to characterize the health of the sensors. Compared with the MWPCA algorithm, it was shown that our proposed algorithm was more accurate in fault diagnosis and could avoid the problem of missing alarm when two sensors had consistent faults, which would provide strong support for the safe operation of the SDR and could further promote its application in long-endurance aircrafts.

1. Introduction

The SDR gas flow regulation technology can realize the adjustable thrust of the aircraft, which is very important to realize the wide envelope and large maneuvering flight of the aircraft [1]. Adjusting the gas flow by controlling the throat area is the most practical flow adjustment scheme. Because the gas flow at high temperature and high pressure is difficult to measure directly, the gas flow is often indirectly regulated by adjusting the pressure in the GG. However, on the one hand, the pressure sensors in the GG face a high-temperature environment (when the pressure inside the GG is 1 Mpa, the temperature can reach 1000 degrees Celsius); on the other hand, the gas pipes of the sensors are easily blocked by the solid powder produced by the combustion of the propellant; there is a certain risk of failure. Therefore, the FDI of the GG can enhance the safety and reliability of the SDR, which is important to guarantee the stable flight of the aircraft.

After decades of research, scholars had proposed a variety of fault diagnosis methods, which could be roughly divided into data-driven approaches, model-based approaches, and knowledge-based approaches [2–4]. Among them, the data-driven approaches usually do not rely on accurate mathematical models, but directly extract the latent information from historical data sets [5]. Therefore, the data-driven approaches were mostly used in sensors' FDI, such as the PCA methods [6–8], time-frequency analysis methods [9, 10], machine learning-based methods [11–17], and the combination of the above methods [18–22]. Huang et al. defined the isolation index by setting each sensor in turn as a missing variable and then recalculating the corresponding fault detection statistic. The missing variable associated with the maximum isolation index was identified as the faulty sensor, and the results showed that the method is effective in detecting and isolating drift faults [6]. In addition, PCA algorithm-based fault diagnosis has been used for FDI in electric traction systems and air-conditioning systems [7, 8], while the PCA methods were

usually completed under the assumption that "only one sensor fails at the same time," which limited the application to some extent. The CIBL-RTCSA (conditionally independent Bayesian learning-based recursive transformed component statistical analysis) approach was proposed in reference [9], and the accuracy of FDI could be effectively improved compared with the naive Bayes. In reference [10], for the problem of motor fault diagnosis, the Fourier decomposition of the Hilbert modulus obtained by different measurement methods was performed to enhance the expression of its characteristic quantity, which could improve the accuracy of fault diagnosis. Obviously, the methods based on time-frequency analysis were usually used for offline FDI due to their large computational load and dependence on a large amount of sample data. Souza et al. used a predictive maintenance model with convolutional neural network (PDM-CNN) to classify bearing faults, and the validation based on a publicly available database showed that the model was more than 97% accurate in classifying faults [11]. Mousavi et al. employed fuzzy inference to estimate the severity of faults based on fuzzy rules extracted from fault patterns and used adaptive thresholds to improve the accuracy of fault estimation [12]. Toscano and Lyonnet presented a parametrization method of a fuzzy classifier from a set of examples without necessarily using a process of iterative training, and this classifier was applied to the diagnosis of a DC motor showing its effectiveness [13]. Jan et al. used a fuzzy deep neural network (FDNN) for diagnosing sensor fault types, while a support vector machine (SVM) was used for fault classification, and the fault detection performance was analysed from several aspects utilizing fault simulation and injection [14]. Saeed et al. have used the Extremely Randomized Trees method to solve the problem of fault diagnosis of wireless sensor network, and it has been shown that this method had strong robustness to signal noise [15]. Siahpour et al. adopted a deep learning-based cross-sensor domain adaptation approach for machinery fault diagnosis, which can achieve 95% diagnostic accuracy [16]. Based on a multilabel classification algorithm, Tan et al. used a single fault data for simultaneous fault diagnosis, which significantly reduced the requirements for training data in machine learning. However, he also pointed out that the algorithm is difficult to deal with the problem of data imbalance [17]. And Lei et al. also pointed out that intelligent fault diagnosis based on machine learning still relies on expert knowledge; although deep learning can automatically learn features, it requires enough labelled samples, which are impractical in engineering scenarios [23].

In summary, both time-frequency analysis and machine learning-based methods rely heavily on sample data, which often leads to large and complex computations in their applications. However, the PCA methods could describe high-dimensional data with fewer principal elements and realize "data dimensionality reduction," thereby greatly reducing the amount of data calculation, which is its significant advantage. Therefore, the PCA methods were often used in combination with the other two methods for FDI. Rezamand et al. applied a wavelet-based probability density function (PDF) to obtain the probability of maintaining health from the extracted principal components (PCs) and finally predicted the remaining useful life of the wind turbine using the Bayesian algorithm and illustrated the effectiveness of the proposed method through experimental tests [18]. For wind turbine systems, Fu et al. used the uncorrelated multilinear principal component analysis (UMPCA) to extract uncorrelated principal components from measurement data on the one hand and used the fast Fourier transform (FFT) to enhance the data classification capability of UMPCA on the other hand, illustrating the more effective fault classification capability of the proposed algorithm by comparing it with the multilinear principal component analysis (MPCA) method [19]. Kordestani et al. used the DPCA algorithm to reduce the data dimension of the vibration signal and used the support vector machine (SVM) to detect and isolate the gear faults in wind turbines. The analysis of the historical data has indicated the effectiveness of the algorithm [20]. And Li and Qu combined the convolutional neural network (CNN) and PCA methods to solve the problem of aeroengine sensors fault diagnosis, which could improve the efficiency of CNN and the accuracy of fault diagnosis [21]. A novel CNN with the function of spectrum calculation and fault diagnosis was designed, in which the spectrum calculation network and the fault diagnosis network were connected in series. Only by system input and output, the fault diagnosis could be realized, which avoided the complex process in traditional methods [22]. However, the data-driven approaches still need sufficient fault data for support and often have poor real-time performance, making it difficult to complete online FDI tasks.

The model-based approaches have clear physical meanings and are important research directions for sensors' FDI, such as the FDI of sensors based on reference models as well as residuals, but are significantly affected by the process' disturbance model estimation [24]. Jiang et al. used the Dempster-Shafer evidence theory to establish the fault model and test model of the sensors, which could better express the uncertainty information and fit the measurement data [25]. In addition, the observer-based method can also be attributed to one of the model-based methods, for example, the adaptive neural network observer and the unknown input observer methods were used in the references [26, 27], respectively. However, in practical applications, the research objects often have many dynamic characteristics that are not easy to model, which also face many disturbances in the working process, so the mismatch of the models may lead to serious misclassification.

The knowledge-based approaches are far from perfect due to limited knowledge, single repeatability of rules, and subjectivity of function definition [2], while they were usually used in combination with data-based and model-based methods [8, 26]. The above three approaches have their own advantages, for example, the model-based approaches have clear physical meaning but are affected by the uncertainty of the models. Although the data-driven approaches do not require accurate models, they rely on the historical data of the systems, while the knowledge-based approaches to fault diagnosis are highly accurate but have knowledge bottlenecks and are less versatile [3]. Therefore, it is worthwhile to focus on one of the research directions to reasonably and comprehensively apply various

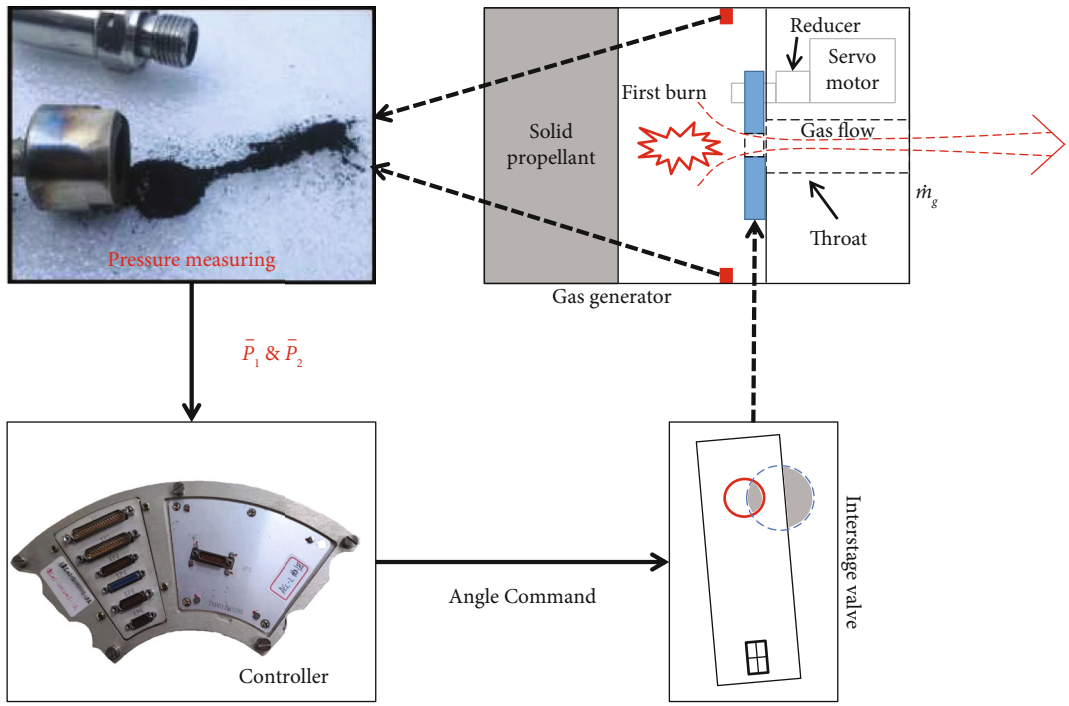

Figure 1: The structure and working principle of the GG.

approaches to improve the accuracy of FDI and enhance the fault tolerance performance of aircraft [28].

Some scholars had realized that when there were multiple data sources representing the same variable, a metric was needed to measure the difference between different pieces of evidence. For example, Ji et al. performed initial fault detection based on augmented the Mahalanobis distance, but this method required a priori knowledge of fault direction information [29]. Based on the classic Dempster-Shafer evidence theory, Lin et al. used the Euclidean distance to characterize the difference between different pieces of evidence, which could better analyse the conflict between them [30]. Similarly, Xiao also used the Dempster-Shafer evidence theory to characterize conflicts between pieces of evidence [31]. Compared with the classical Euclidean metric, the gap metric can be used to measure the correlation of different data in high-dimensional space, but the application of the gap metric theory to the fault diagnosis of sensors was rarely studied. Zhou proposed a new framework of fault diagnosis and fault-tolerant control based on gap metric, which has important guiding significance for the application of gap metric theory in fault diagnosis [32]. Wang et al. used the gap metric to perform fault detectability analysis for systems with model uncertainty and external disturbances and illustrated the effectiveness of the proposed method using a classical case [33]. In the reference [34], a data-driven gap metric was used to design a suitable fault cluster to improve the separability of initial faults. In addition, the gas flow regulation system of SDR is a closed-loop system. Compared with the open-loop system, the fault diagnosis performance of the closed-loop system is mainly degraded; on the one hand, the control quantity will cover up the smaller faults, and on the other hand, the feedback control may make the fault propagate in the system [35]. Zhou had pointed out that the complex impact of closed-loop feedback on fault diagnosis has not been fully analysed, and further research was needed [36]. For the GG system, due to the limited installation space of the pressure sensors and the cost of the SDR, too much sensor redundancy is usually not used. Even if multiple (more than 2) sensors are used to measure the pressure in the GG at the same time, although the faulty sensors can be isolated by the "voting method" (It is assumed that the failure of several sensors at the same time is a small probability event, so the sensor whose measured values differs from the others is considered a faulty element), however, there is still a problem, that is, when there are only two sensors left in the system working normally (assuming that the remaining sensors have been isolated), the "voting method" cannot continue to perform FDI.

This paper mainly aimed at the GG system of SDR with double pressure feedback and combined gap metric, PCA, and Kalman's principle to diagnose and isolate the fault of the pressure sensors. The main contributions of this paper are as follows:

(a) Based on PCA theory, a "consistency index" was constructed, which could ensure the monotonicity under fault conditions and the convergence under nonfault conditions, so the fault detectability was improved

(b) Based on the Kalman principle, the pressure in the GG was estimated by using the redundant information of the system, and the phase lead correction and tracking differentiator (TD) were designed to reduce the noise and delay, which could improve

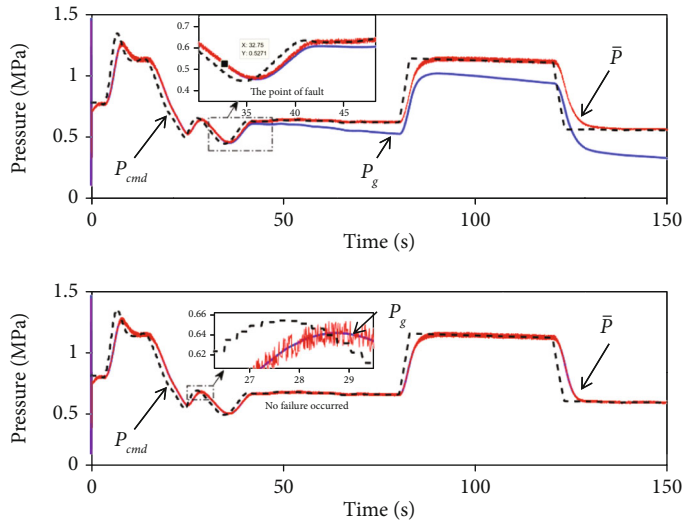

Figure 2: Influence of closed-loop control on fault diagnosis.

the accuracy and real-time performance of the estimation

(c) The gap metric between the measured pressure and the estimated pressure was employed to characterize the health of the sensors, and an FDI algorithm for GG with double pressure feedback was proposed

The rest of this paper was organized as follows: In Section 2, the working principle of the GG was introduced, the failure model of the sensors was developed, and the effect of sensor failure on the closed-loop system was also analysed. The FDI algorithm for pressure sensors was presented in Section 3, which made comprehensive use of Kalman's principle, gap metric, and PCA theory with corresponding improvements. In Section 4, several simulations were performed for the case of one pressure sensor failure or two pressure sensors failing at the same time. Finally, the conclusion and outlook were given in Section 5.

2. Types of Pressure Sensor Failures and Their Impact on the GG

2.1. The Working Process of the GG. As shown in Figure 1, when the propellant in the GG burns to generate gas, the controller will collect the pressure data in the GG through the pressure sensors, and according to the gas flow required by the system, the control angle of the interstage valve will be calculated, so that the purpose of regulating the pressure in the GG and indirectly controlling the gas flow rate could be achieved. In the GG system studied in this paper, there are two sensor measurement points, and under normal conditions, the GG's pressure measured at the two measurement points is approximately equal. The average of the two measurements at each moment is used as the feedback for closed-loop flow regulation.

2.2. Failure Model of Pressure Sensors. For pressure sensors, the fault types can be roughly divided into deviation faults (The faulty measurement differs from the correct measurement by a certain constant), complete failures (The measured value does not change with the actual change, and always maintains a certain value), drift faults (The degree of failure varies linearly with time), and precision degradation faults (The average error of the measured value increases). The first two of the above faults can be considered as sudden faults, which are usually easier to diagnose, while the last two can be considered as slow faults, which are relatively more difficult to diagnose. Therefore, this paper mainly aims at diagnosing and isolating the slow fault of the sensors. For drift faults, the mathematical model can be expressed by Equation (1), and the failure of precision degradation can be expressed by Equation (2) [37].

$$\bar{P}(t) = p_g(t) + \eta + d(t - t_s), \tag{1}$$

$$\bar{P}(t) = p_g(t) + \eta + \eta^*, \tag{2}$$

where $\bar{P}(t)$ is the measured value of the sensor, d is a constant, t_s is the moment when the fault occurs, $p_g(t)$ is the true value of the pressure in GG, and η is the measurement noise, which can be assumed to obey the $N(0, {\sigma_1}^2)$ distribution. As well as η^* is the newly added error in the failure of precision degradation, which can be considered to obey the $N(0, {\sigma_2}^2)$ distribution.

2.3. Effects of Sensor Failure on Closed-Loop Systems. Under the influence of the closed-loop control system, the "correction" ability of the control law will cover the "fault information". As shown in Figure 2, when no fault occurred, the system always maintained $\bar{P} \approx p_g$; however, when a fault occurred, the situation became different. It was assumed that at 32.75 seconds, the pressure sensors had a slow drift fault ($d_1 = d_2 = 0.002$); it could be seen that under the closed-loop control and the regulation of the interstage valve, although the measured value ($\bar{P}$) could still follow the command (P_{cmd}) well, but in fact, the true value (P_g) of the

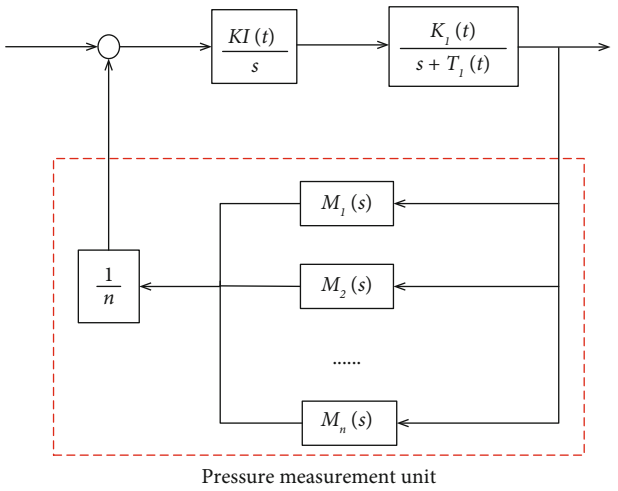

FIGURE 3: Multisensor redundant closed-loop control system for GG's pressure.

system responded in the opposite direction of the fault, and the longer the drift fault occurred, the greater the deviation of $\bar{P}$ from P_g, and the greater the damage to the system.

2.4. Influence of Sensor Failure on the Stability of Closed-Loop System. It is assumed that multiple sensors are used to measure the pressure of GG at the same time, and the average of their measured values is used as the feedback. The mathematical model of GG can be equivalent to a first-order system [38]. For the convenience of analysis, the control law adopts the integral link; $M_n(s)$ represents the transfer function of the pressure sensor (As shown in Figure 3). As we have known, under ideal conditions, the transfer function of each pressure sensor is 1. When there are measurement noise and faults, the transfer function of the measurement unit can be regarded as $K(t)$; then, the closed-loop transfer function of the system was shown in Equation (3).

$$G_{\mathrm{cl}}(s) = \frac{\mathrm{KI}(t) \bullet K_1(t)}{s^2 + T_1(t) \bullet s + K(t) \bullet \mathrm{KI}(t) \bullet K_1(t)}, \tag{3}$$

where $K(t) = 1 + (\sum_{i=1}^{n}(\eta_i + \xi_i)/n \bullet p_g)$, $\xi(t) = d(t - t_s)$.

For this system, it is clear that $K_1(t)$, $T_1(t)$, and $KI(t)$ are all positive values (It has been described in reference [38]), so the root's polarity of the characteristic equation can be judged according to Veda's theorem (When the sum of the two roots is negative and the product of the two roots is positive, both roots of the system will be negative). Then, according to the Hurwitz criterion, the stability condition of the system can be obtained. When $\sum_{i=1}^{n}(\eta_i + \xi_i) > -n \bullet p_g$, the system is stable.

3. Fault Diagnosis Principle and Algorithm

3.1. Construction of the "Consistency Index." The essence of PCA is to find a set of "bases", so that the projection of the original data on this set of "bases" is as centrally as possible. For this system, the two sensors measure the same static variable (GG's pressure), and the measured values of the two sensors can maintain good consistency during normal operation. However, when one of them fails, the consistency will be broken. Since the measurements were updated in real time, we used a moving window to perform principal component analysis (MWPCA) on the two sets of dynamic measurement data. In this way, the "consistency" of them could be judged and evaluated. The general process of PCA was shown in Figure 4.

For this system, the data acquisition matrix of the two sensors in the moving window length k may be expressed by Equation (4), and the moving step size of the window is d, which can be expressed by Equation (5). For the Step 4 in Figure 4, the traditional calculation method was shown by Equation (6).

$$X(t) = \begin{bmatrix} \bar{P}_1(t-k+1) & \bar{P}_2(t-k+1) \\ \bar{P}_1(t-k+2) & \bar{P}_2(t-k+2) \\ \cdots & \cdots \\ \bar{P}_1(t) & \bar{P}_2(t) \end{bmatrix}_{k\times 2}, t > k, \tag{4}$$

$$X(t+d) = \begin{bmatrix} \bar{P}_1(t-k+1+d) & \bar{P}_2(t-k+1+d) \\ \bar{P}_1(t-k+2+d) & \bar{P}_2(t-k+2+d) \\ \cdots & \cdots \\ \bar{P}_1(t+d) & \bar{P}_2(t+d) \end{bmatrix}_{k\times 2}, \tag{5}$$

$$[\mathrm{PC1}(t)\ \mathrm{PC2}(t)] = X(t) \bullet [P(t)\ \tilde{P}(t)]. \tag{6}$$

The traditional method detects faults through SPE statistics and the relationship between SPE and cl_α. When SPE $\leq \mathrm{cl}_\alpha$, it was judged that a fault occurs [39]. However, it is insensitive to minor sensor faults, which are relatively difficult to detect [6]. For the double pressure feedback system, the effect of the closed-loop control makes Err tend to 0; then, $\bar{P}_1(t)$ and $\bar{P}_2(t)$ are approximately symmetric about P_{cmd}; therefore, when one of the sensors drifts, the actual pressure of the system must respond in the opposite direction. The value of PC2 can well reflect the consistency of the two sets of data. The better the consistency, the closer its value to 0. However, the characteristics of PC2 will be changed under the influence of the closed-loop system.

$$\mathrm{Err} = P_{\mathrm{cmd}} - \frac{1}{2} \bullet [\bar{P}_1(t) + \bar{P}_2(t)]. \tag{7}$$

Therefore, we use Equation (8) to characterize the consistency of the two sensors and refer to P_e as the " Consistency Index ".

$$\mathrm{Pe}(t) = \left| \begin{bmatrix} \min\left(X(t)_{k1}, X(t)_{k2}\right) \\ \max\left(X(t)_{k1}, X(t)_{k2}\right) \end{bmatrix}^{\mathrm{T}} \bullet \begin{bmatrix} \tilde{P}(t)_{11} \\ \tilde{P}(t)_{12} \end{bmatrix} \right|, \tag{8}$$

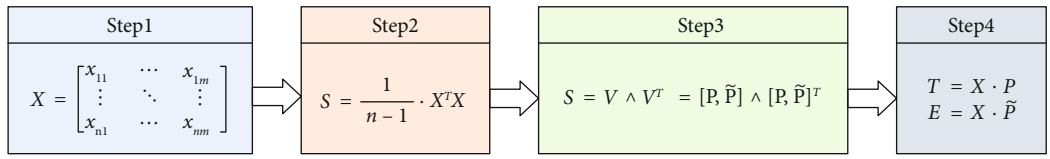

Figure 4: General process of PCA.

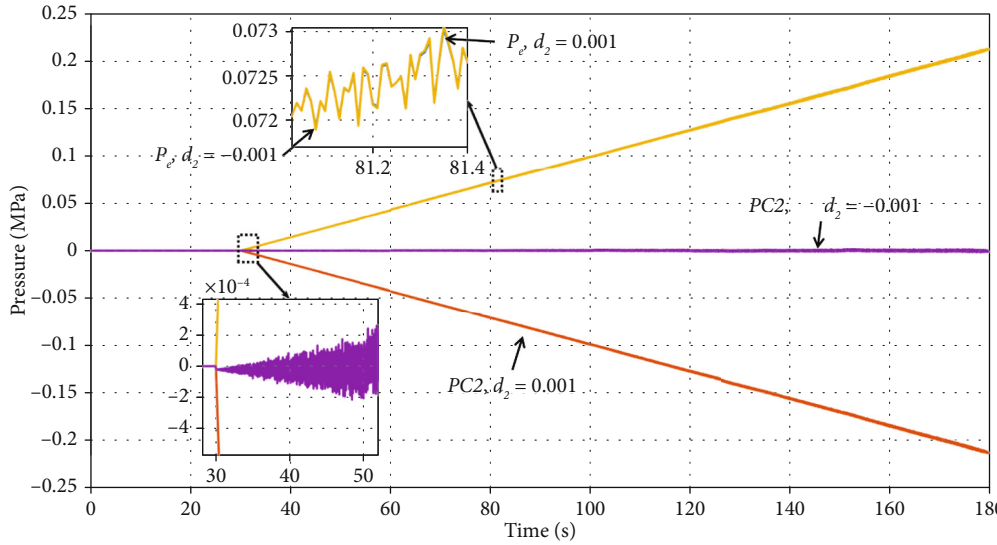

Figure 5: The PC2 and Pe under different fault conditions.

where the subscript "ij" means row i, column j of the matrix, for example, the $X(t)_{k1}$ means the element at row k and column 1 of $X(t)$, the superscript "T" represents the transpose of the matrix, and $|*|$ is the absolute value.

For a $k \times 2$ matrix, when the eigenvalues of its covariance matrix satisfy $\lambda_1 > \lambda_2 \geq 0$, it is easy to obtain $|\tilde{P}(t)_{11}| < |\tilde{P}(t)_{12}|$, so Equation (8) can guarantee the divergence characteristics of P_e when a fault occurs. When there is no fault, $\tilde{P}(t)_{11} \approx \tilde{P}(t)_{12}$, $X(t)_{k1} \approx Y(t)_{k1}$, so it does not affect its convergence (See Part A in the Supplementary Material for more analysis, where Figure S1 is a visual illustration of Part A). As shown in Figure 5, when $d_2 = 0.001, d_1 = 0$, the second principal element calculated by the two methods was symmetric about $x = 0$, and there was no difference after taking the absolute value. However, when $d_2 = -0.001$, the PC2 and Pe were quite different, while the Pe still maintained the good monotonicity. (As shown in Table 1)

3.2. Gap Metric and the Sensor's Health. The geometric meaning of the gap metric between two real numbers is their chord distance after projection on the unit of Riemann's sphere. Compared with the Euclidean metric, it can highlight the correlation between different variables, as shown in Equation (9). For example, when $\bar{P}_1(t_1) = 1$ MPa, $\bar{P}_2(t_1) = 1.5$ MPa, then $\Delta\bar{P}(t_1) = \bar{P}_2(t_1) - \bar{P}_1(t_1) = 0.5$ MPa, $\delta(\bar{P}_1(t_1), \bar{P}_2(t_1)) \approx 0.196$, and when $\bar{P}_1(t_2) = 4$ MPa, $\bar{P}_2(t_2) = 4.5$ MPa, then $\Delta\bar{P}(t_2) = \bar{P}_2(t_2) - \bar{P}_1(t_2) = 0.5$ MPa, $\delta(\bar{P}_1(t_2), \bar{P}_2(t_2)) \approx 0.026$, obviously $\Delta\bar{P}(t_1) = \Delta\bar{P}(t_2)$, but $\delta(\bar{P}_1(t_1), \bar{P}_2(t_1)) > \delta(\bar{P}_1(t_2), \bar{P}_2(t_2))$. In fact, the gap metric could cover both the amount and the rate of change under the Euclidean metric.

$$\delta(p_1, p_2) = \frac{|p_1 - p_2|}{\sqrt{1 + |p_1|^2} \bullet \sqrt{1 + |p_2|^2}}. \tag{9}$$

For this system, we used the gap metric between the measurement ($\bar{P}$) and the estimate pressure ($\hat{P}$) to measure the health of the sensor. And the difference in the health of the two sensors can better reflect the relative health status between the two sensors, which are conducive to fault detection, as shown in Equation (10). When the sensors work normally, $\hat{P} \approx \bar{P}$, H_1, or H_2 is close to 0, while when there is a fault, $\hat{P} \neq \bar{P}$, the health status deteriorates, and the worse the health status is, the closer H_1 or H_2 is to 1. H_m is used to indicate the cumulative amount of health difference between two sensors, and the larger H_m indicates the greater health difference between two sensors, $H_m \in [-\infty, +\infty]$, while $H_1 \& H_2 \in [0, 1]$.

$$\begin{cases} H_m = \int_0^t (H_1 - H_2) \bullet \mathrm{dt}, \\ H_1 = \delta\left(\frac{\hat{P}}{\hat{P} + \bar{P}_1}, \frac{\bar{P}_1}{\hat{P} + \bar{P}_1}\right), \\ H_2 = \delta\left(\frac{\hat{P}}{\hat{P} + \bar{P}_2}, \frac{\bar{P}_2}{\hat{P} + \bar{P}_2}\right). \end{cases} \tag{10}$$

As shown in Figure 6 (The double vertical axis legend was used here, where H_1 and H_2 correspond to the vertical axis on

Table 1: Under closed-loop control, the characteristics of PC2 and Pe are compared.

d_1	d_2	η_1	η_2	PC2(t)	Pe(t)
0.001	0	0.2%	0.2%	Nonmonotonicity	Monotonicity
-0.001	0	0.2%	0.2%	Monotonicity	Monotonicity
0	0.001	0.2%	0.2%	Monotonicity	Monotonicity
0	-0.001	0.2%	0.2%	Nonmonotonicity	Monotonicity
0	0	0.2%	2%	Nonmonotonicity	Nonmonotonicity

the right side of the figure, and H_m corresponds to the vertical axis on the left side of the figure), at the 30th second, $\bar{P}_1$ has a drift fault, $d_1 = -0.001$, $d_2 = 0$, H_1 and H_2 are approximately equal before the fault occurs ($H_1 \approx H_2 \approx 0$). After the fault occurred, H_1 and H_2 gradually differed, the H_1 increased with time, reaching about 0.32 at the 300th second, and correspondingly, the H_m also rose rapidly and eventually reached around 32. Similarly, if a drift fault occurs in $\bar{P}_2$, H_m will drop rapidly, and when the fault is isolated, H_m will be less than zero.

3.3. Kalman's Filter Algorithm for Measurement Delay. For the problem of fault diagnosis, we should focus on the redundant information in the system and use them as the evidence of fault diagnosis. From the Equation (11) of the GG, (See Part B in the Supplementary Material for a detailed derivation process) the steady-state pressure in the GG is independent of the free-volume but only related to the throat area (Assuming no change in propellant parameters). And because the valve angle directly reflects the change of the throat area, the valve angle is redundant information that can be used. In GG system of the SDR, the valve angle can be measured in real-time, we can roughly calculate the ΔP_g using the $\Delta\theta$.

$$\frac{dP_g}{dt} = \frac{R_g \cdot T_g}{V} \cdot \left(\rho_b \cdot A_b \cdot a \cdot {P_g}^n - \frac{P_g \cdot A_t}{C_r}\right), \tag{11}$$

where P_g is the gas pressure in GG, R_g is the gas constant, T_g is the gas temperature, and V represents the free-volume, which means the volume between the propellant end face and the throat. ρ_b represents the propellant density, A_b represents the burning area of the propellant, a represents the propellant combustion rate coefficient, n represents the pressure index, A_t represents the throat area, C_r represents the characteristic velocity of the gas, and θ represents the swing angle of the interstage valve.

In addition, the pressure of the GG ultimately affects the pressure of the ram combustor (RC), and the pressure of the RC and the flight conditions (height, Mach, attack angle, sideslip angle) jointly determines the thrust and the axial overload. Therefore, the measured value of the overload sensor is another piece of redundant information that can be used. However, there is usually a certain time delay between the axial overload and the pressure of the GG. Taking a ground test of our research group as an example, by observing the time delay between the pressure response of the GG and the RC, the time delay between the pressure of the GG and the axial overload of the aircraft was indirectly equivalent (Ignore the time delay between the pressure response of the RC and axial overload). As shown in Figure 7, the moment of pressure rise was selected as the observation point, so there was a delay of about 0.8 seconds between the pressure response of GG and RC.

For the time delay problem, a tracking differentiator with lead correction was introduced here. On the one hand, the time delay could be reduced, and on the other hand, the noise caused by the overload measurement could also be reduced. The corresponding algorithm was shown in following equations:

$$\begin{cases} \text{fh} = \text{fhan}(v_1(t-1) - f(N_x, H, \text{Ma}, \text{alpha}, \text{beta}), v_2(t-1), r_0, h_0), \\ v_1(t) = v_1(t-1) + h \cdot v_2(t-1), \\ v_2(t) = v_2(t-1) + h \cdot \text{fh}, \\ P_x(t) = v_1(t) + h \bullet \alpha \bullet v_2(t), \end{cases} \tag{12}$$

$$\begin{cases} d = r_0 \cdot {h_0}^2, a_0 = h_0 \cdot x_2, y = x_1 + a_0, \\ a_1 = \sqrt{d \cdot (d + 8 \cdot |y|)}, \\ a_2 = a_0 + \text{sign}\,(y) \cdot \dfrac{(a_1 - d)}{2}, \\ s_y = \dfrac{[\text{sign}\,(y+d) - \text{sign}\,(y-d)]}{2}, \\ a = (a_0 + y - a_2) \cdot s_y + a_2, \\ s_a = \dfrac{[\text{sign}\,(a+d) - \text{sign}\,(a-d)]}{2}, \\ \text{fhan} = -r \cdot \left[\dfrac{a}{d} + \text{sign}\,(a)\right] \cdot s_a - r_0 \cdot \text{sign}\,(a), \end{cases} \tag{13}$$

where $f(N_x, H, \text{Ma}, \text{alpha}, \text{beta})$ is the function of calculating the pressure of the GG from the overload and flight conditions, the N_x is the axial overload of the aircraft, the v_1 and v_2 are the tracking and differential tracking signals of the input signal, respectively, the α is the correction coefficient, and the P_x is the output of the transition process.

Then, we could use the Kalman information fusion algorithm to obtain the "estimated pressure" according to the valve angle and axial overload and make further preparations for FDI (Equations (14)–(18)). It was assumed that there would be a large error in calculating the pressure of GG (P_g) from the overload information (P_x). Therefore,

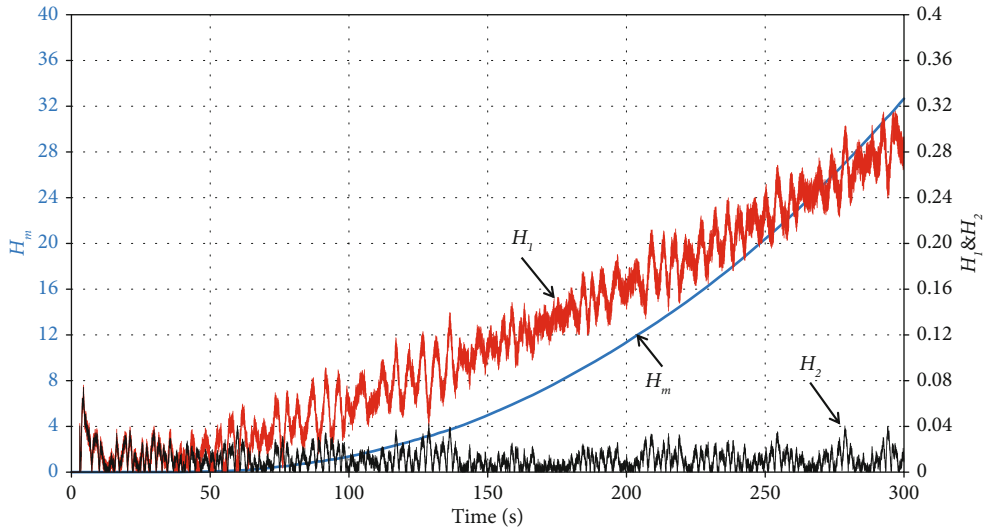

Figure 6: Variation trends of H and H_m when $\bar{P}_1$ had a drift fault.

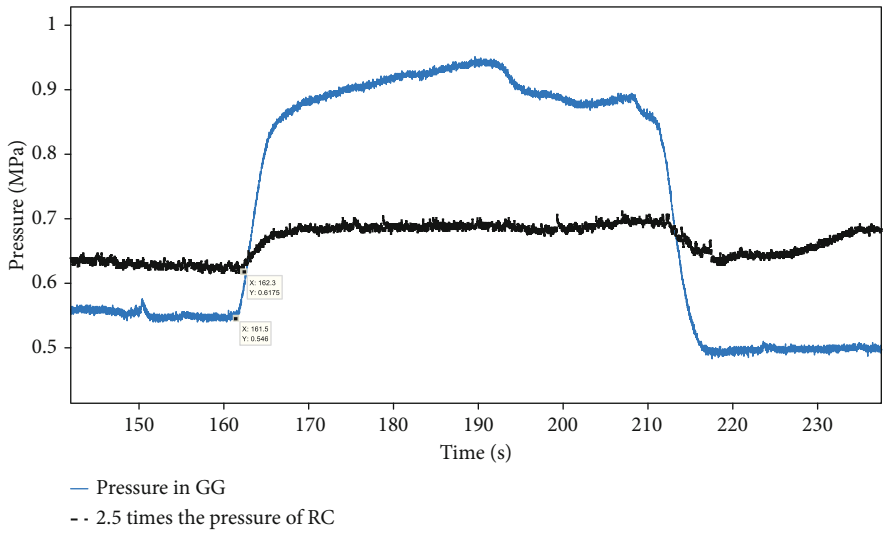

Figure 7: The time delay between the pressure response of the GG and the RC.

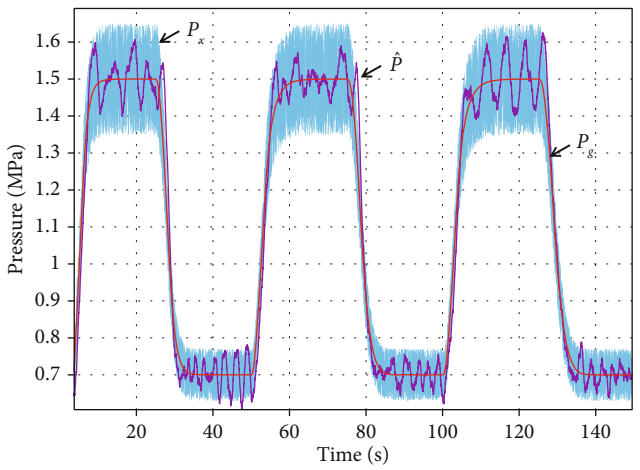

Figure 8: Pressure estimation of GG based on Kalman's principle.

using the Kalman principle to fuse P_x and the valve angle to optimally estimate the pressure ($\widehat{P}$) would not be particularly ideal but would contain large errors. Figure 8 could reflect the relationship among $\widehat{P}$, P_x, and P_g.

$$P_k(t) = \widehat{P}(t-1) + f(\Delta\theta), \tag{14}$$

$$P_A^-(t) = P_A(t-1) + Q_A, \tag{15}$$

$$K(t) = \frac{P_A^-(t)}{[P_A^-(t) + R]}, \tag{16}$$

$$\widehat{P}(t) = P_k(t) + K(t)\bullet[P_x(t) - P_k(t)], \tag{17}$$

$$P_A(t) = [1 - K(t)]\bullet P_A^-(t), \tag{18}$$

where $\Delta\theta$ is the variation of the valve angle, Q_A is the variance when the pressure is calculated from the valve angle,

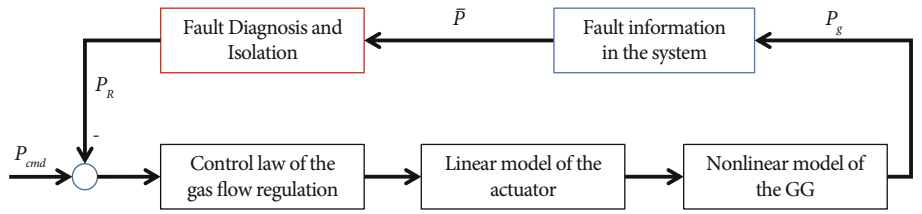

Figure 9: Control schematic with fault diagnosis and isolation algorithms.

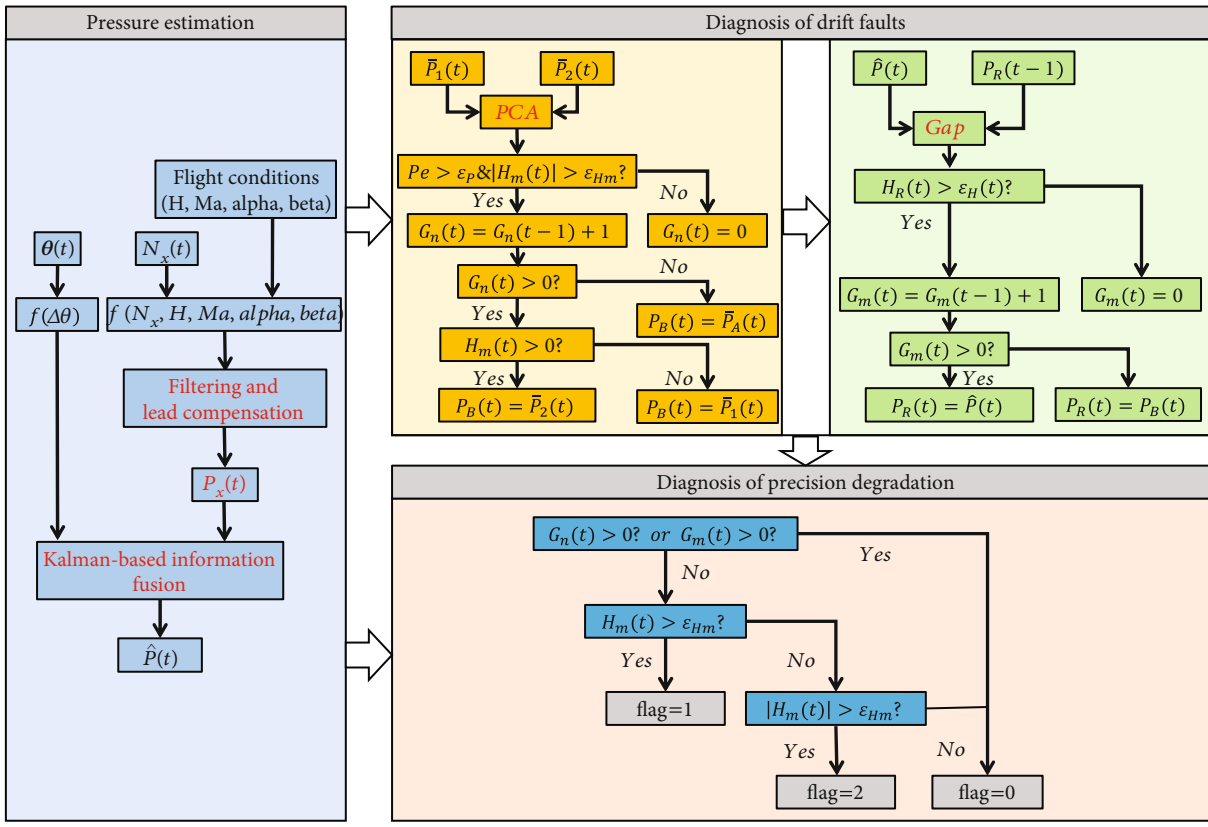

Figure 10: Principles of fault diagnosis and isolation algorithms.

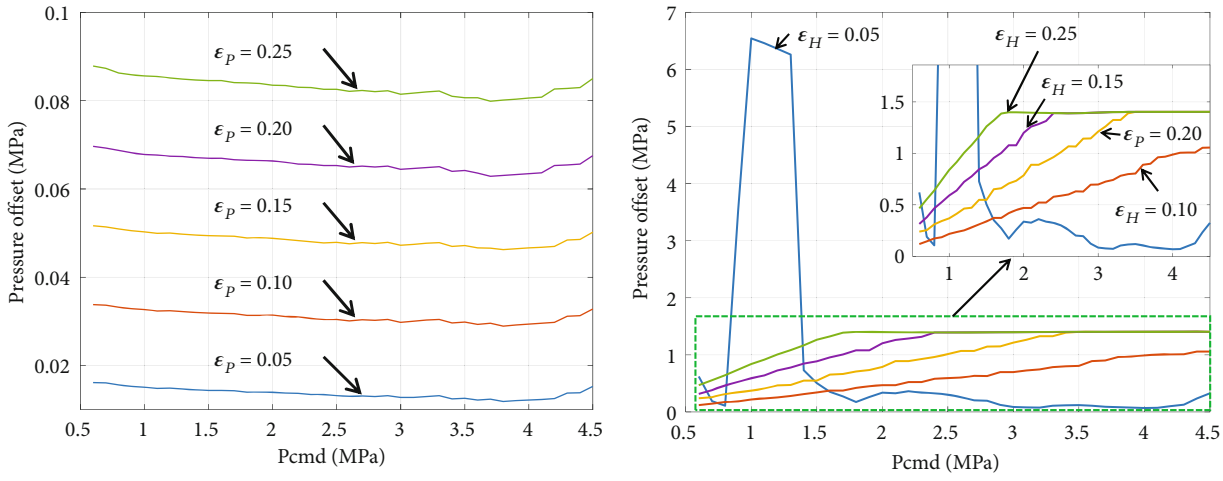

(a) Selection of ε_P

(b) Selection of ε_H

Figure 11: Selection of thresholds for sensor fault isolation.

Table 2: Simulation conditions.

Parameters	Physical meaning	Value	Unit	Parameters	Physical meaning	Value	Unit
r_0	Parameters in the fhan function	0.3	/	Q_A	The variance when estimating pressure from θ	0.01	MPa^2
α	Correction coefficient	100	/	R	The variance when estimating pressure from N_x	0.01	MPa^2
τ	Delay in estimating pressure from N_x	100* h	s	h	The sampling period	0.01	s
ε_{Hm}	Precision degradation monitoring threshold	0.01	/	h_0	Parameters in the *fhan* function	0.01	/
ε_P	Individual sensor isolation thresholds	0.1	/	ε_H	Both sensors isolation thresholds	0.1	/
η	The measurement noise	0.2%	/	η^*	The newly added error in the failure of precision degradation	0.8%	/

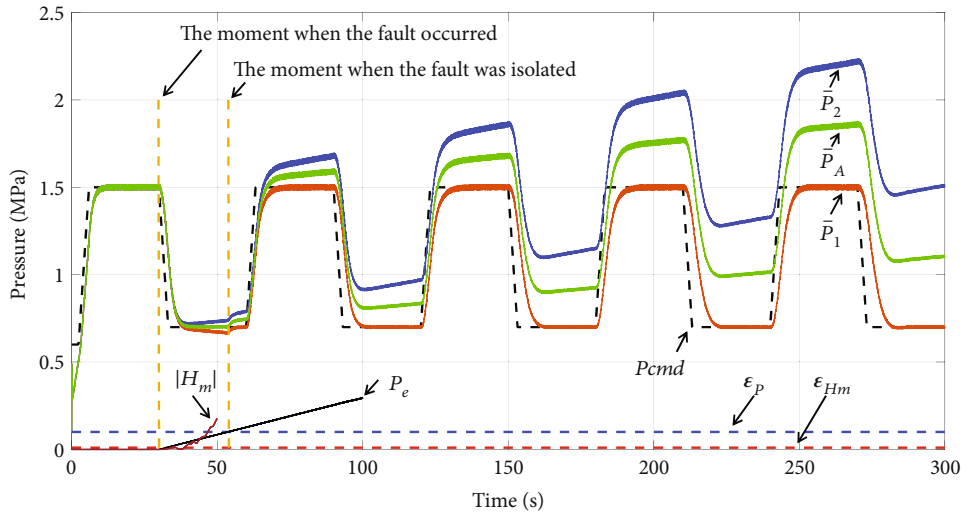

Figure 12: Only one of the pressure sensors was faulty.

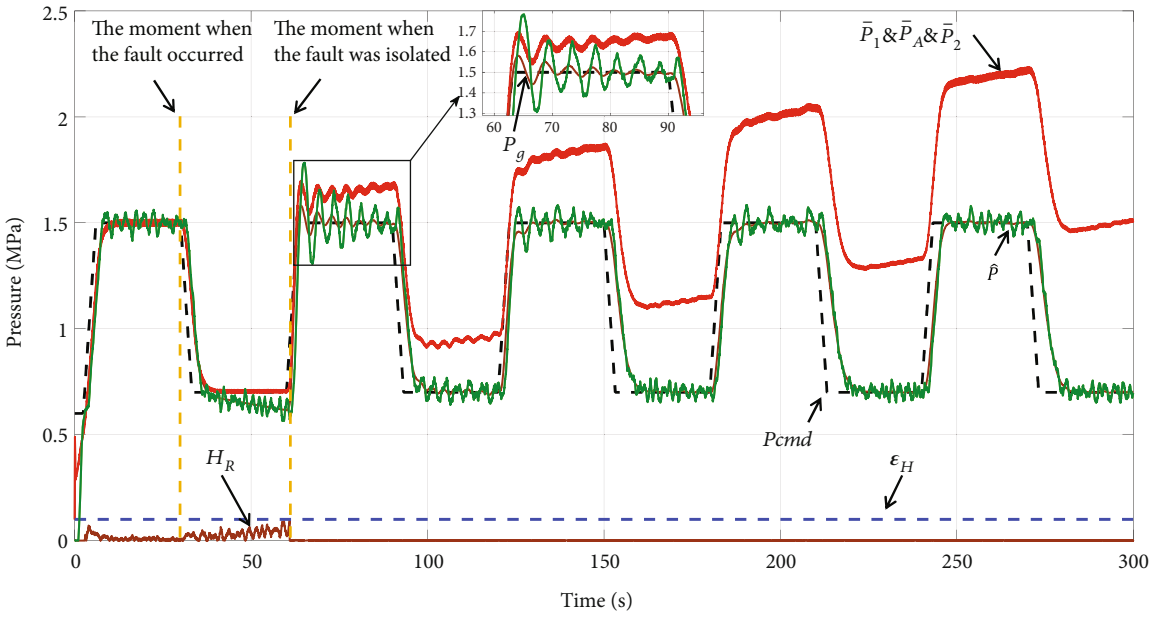

Figure 13: Both sensors fail with the same drift trend.

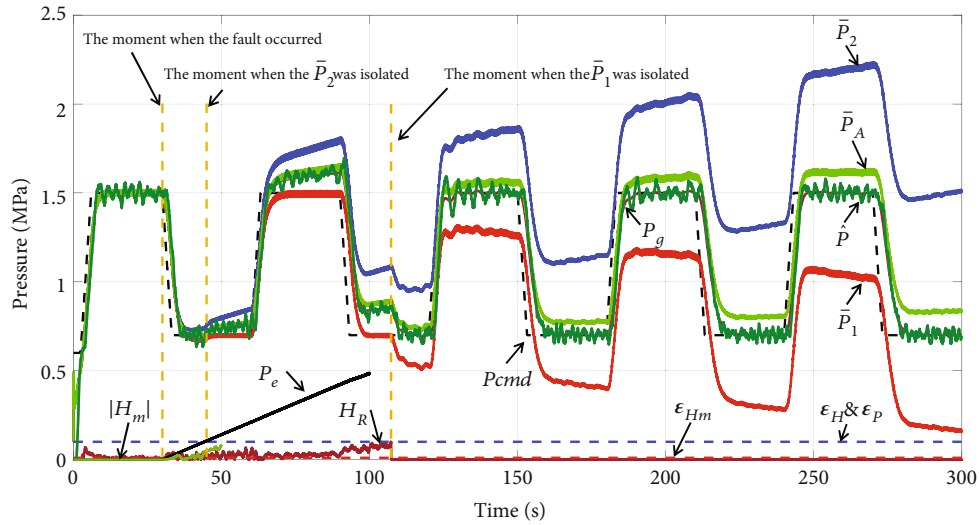

Figure 14: Drift failure with inconsistent trend between two sensors.

Table 3: Statistics of simulation results.

Fault type	The total number of simulations	The algorithm proposed in this paper			MWPCA-SPE		
		Missing alarm	False alarm	Accuracy	Missing alarm	False alarm	Accuracy
A	400	0	0	100%	6.1%	0	93.9%
B1	400	0	0	100%	100%	0	0
B2	400	0	0	100%	7%	0	93%
C1	400	1.25%	3%	95.8%	8.2%	0	91.8%
C2	400	1.25%	3%	95.8%	8.2%	0	91.8%

Remark: the "Fault Type A" means only one of the pressure sensors was drift faulty, the "Fault Type B1" means both the pressure sensors were drift faulty, and $d_1 = d_2 = d$, the "Fault Type B2" means $d_2 = \mathrm{d}$, $d_1 = d/2$. The "Fault Type C1" means precision degradation faults, and $\eta_1 = \eta_2 = \eta = 0.2\%$, $\eta_1{}^* = 0$, $\eta_2{}^* = \eta^*$, the "Fault Type C2" means $\eta_1 = \eta_2 = \eta = 0.2\%$, $\eta_1{}^* = \eta^*$, $\eta_2{}^* = 0$.

and R is the variance when the pressure is calculated from the axial overload.

3.4. Fault Isolation Algorithm. How the FDI works in the control system had been represented in Figure 9, and the detailed principle inside the red box would be illustrated in Figure 10. The blue box represented the fault information of the system. In this paper, the fault was simulated based on the mathematical model. Firstly, based on the redundancy of N_x and θ, the Kalman principle was used to optimally estimate the pressure in the GG, which was $\hat{P}$ in Figure 10. Secondly, the P_e was used to evaluate the consistency of the two pressure sensors' measured values (In order to reduce the probability of misdiagnosis, H_m was also used to assess the difference in health between the two sensors, that is, the consistency of the measured values). And when it was poor, the H_m would be used to judge which sensor should be isolated. Since it was possible to maintain good consistency when both sensors failed, the H_R could be used to judge whether to isolate the two sensors at the same time. The definition of H_R was shown in Equation (19).

In addition, the polarity of H_m and its relationship with the corresponding threshold could be used to determine which sensor had lower accuracy. When H_m or its absolute value exceeds the threshold value, it is determined that a precision degradation fault occurs. When "Flag = 1," it means that the precision degradation occurs in $\bar{P}_1$, and when "Flag = 2," it means that the precision degradation occurs in $\bar{P}_2$. Since such faults are relatively less harmful to the closed-loop system, only the monitoring function was performed here. In addition, when two kinds of faults (drift fault and precision degradation fault) occur simultaneously, only the drift fault is recognized, and the accuracy monitoring function is performed when there is no drift fault.

$$H_R = \delta\left(\frac{\hat{P}}{\hat{P} + P_R}, \frac{P_R}{\hat{P} + P_R}\right). \tag{19}$$

From Figure 11(a), it could be seen that when the fault was isolated, the pressure offset due to different ε_P (when $d_1 = d_2 = 0.003$). If the ε_P was too large, the fault diagnosis process will be too long, and if the ε_P was too small, the diagnosis algorithm will be too sensitive and cause misdiagnosis. If $\varepsilon_P = 0.1$, when the fault was isolated, the deviation between the measured pressure and the real pressure would be within 0.04 MPa. From Figure 11(b), it could be seen that if ε_H was too small, it was too easy to isolate both sensors. For example,

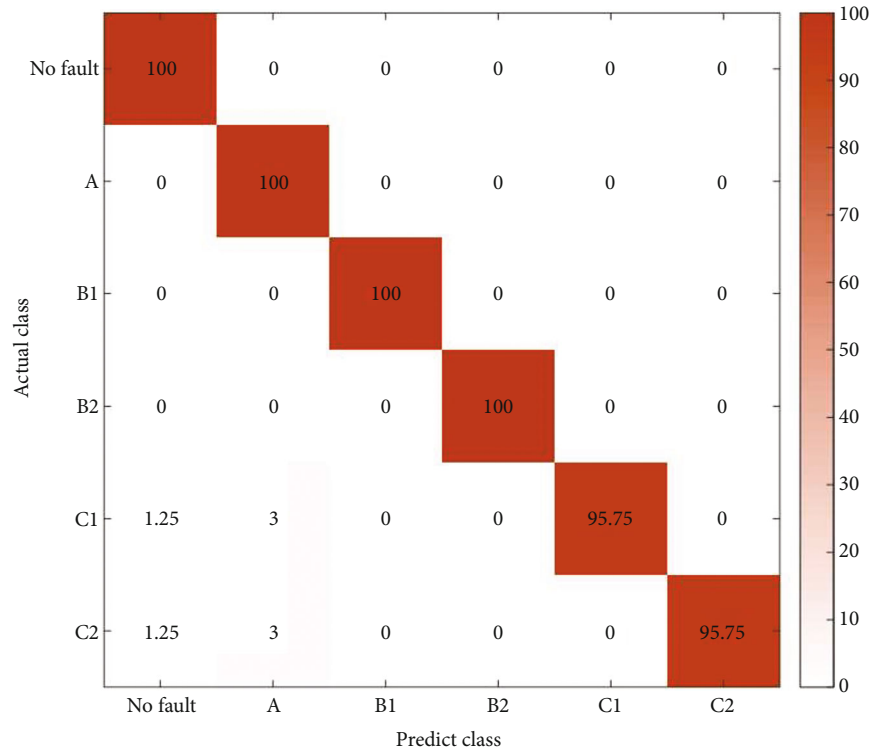

(a) The confusion matrix of the algorithm proposed in this paper

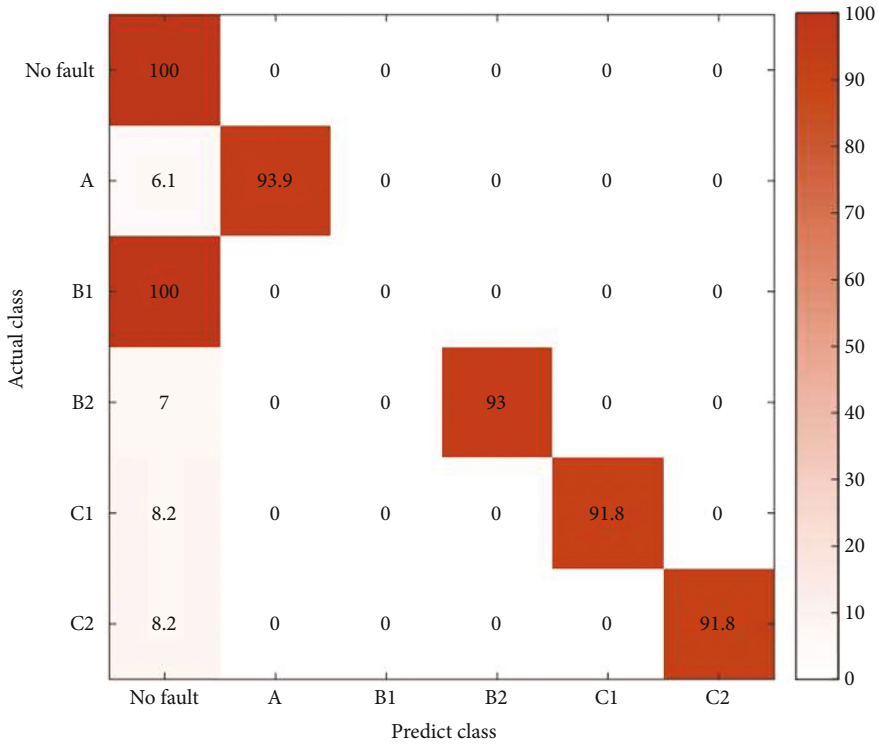

(b) Confusion matrix of MWPCA-SPE

Figure 15: Confusion matrix for fault diagnosis of two algorithms.

when the value was 0.05, the two sensors have been isolated at the beginning of the simulation. But if ε_H was too large, the fault identification will be too slow, which will increase the damage to the system. After comprehensive consideration, we choose ε_H as 0.1; when the pressure command was in the range of 0.6 MPa and 4.5 MPa, the pressure offset was between 0.12 and 1.06 MPa. According to a similar method, $\varepsilon_{\mathrm{Hm}}$ could be taken as 0.01, and the process would not be repeated.

4. Mathematical Simulation and Analysis

In this section, simulations were performed for the cases of one of sensors failure and both sensors failure at the same time, so that the effectiveness of the FDI algorithm in the paper could be fully judged and analysed. Among them, the simultaneous failure of the two sensors includes a failure with the same drift trend and a failure with an inconsistent drift trend. Matlab/Simulink was used as the simulation software, and the simulation conditions were given in Table 2.

4.1. Only One of the Pressure Sensors Is Faulty. We could make $\bar{P}_2$ drift fault from the 30th second, $d_2 = 0.003$, $d_1 = 0$, and the pressure command was a trapezoidal wave command with a slope of 0.25 MPa/s from 0.7 to 1.5 MPa. As could be seen in Figure 12, before the fault was isolated, $\bar{P}_A$ entered the control closed loop as feedback. At 53.62 seconds, $\bar{P}_2$ was diagnosed as a faulty sensor and was isolated; after that, $\bar{P}_1$ alone entered the control closed loop as feedback. And $\bar{P}_1$ reflected the real situation of the system.

4.2. Both Pressure Sensors Are Faulty. It was set that both sensors had drift faults from the 30th second, $d_1 = d_2 = 0.003$, and the pressure command was a trapezoidal wave command with a slope of 0.25 MPa/s from 0.7 to 1.5 MPa. From Figure 13, it could be seen that before the failure, the combined health of the sensors (H_R) varies within a certain range, until the health threshold was exceeded at 61.32 seconds, and both sensors were isolated. After that, closed-loop control was performed using the $\hat{P}$ as the feedback.

It was set that both sensors had drift faults from the 30th second, $d_1 = -0.002$, $d_2 = 0.003$, and the pressure command was a trapezoidal wave command with a slope of 0.25 MPa/s from 0.7 to 1.5 MPa. As shown in Figure 14, at 44.25 seconds, P_e exceeded the threshold firstly, and $\bar{P}_2$ was isolated firstly due to its greater degree of failure. At the 107.4 seconds, the H_R exceeds the threshold, $\bar{P}_1$ was also isolated; after that, closed-loop control was performed using the $\hat{P}$ as the feedback.

4.3. The Accuracy of the FDI. In this section, the accuracy of the FDI algorithm described in this paper was calculated for drift faults and measurement precision degradation faults. For the GG system with double pressure feedback studied in this paper, its FDI algorithm was rarely studied, so this paper adopted the classic MWPCA algorithm and SPE detection method as the control group. Among them, P_{cmd} was taken as a fixed value between 0.6 and 4.5 MPa. For drift faults, the drift rate d was taken as a value between -0.002 and -0.020. For the failure of measurement accuracy decline, η was taken as 0.2%, and the newly added measurement error of the faulty sensor (η^*) was taken as a value between 0.8% and 2.3%. The simulation results were shown in Table 3 (Detailed simulation results were provided in Tables S1-S5 in Part C of the Supplementary Material). For the detection of precision degradation faults, the fault would be missed because the fault was too small, and the P_e and H_m would exceed the thresholds because the fault was too serious, so the faulty sensor was isolated. The situation was classified as a missing alarm in this paper, that is, the precision degradation fault was falsely reported as a drift fault. The confusion matrix of the two algorithms for fault diagnosis was shown in Figure 15. It could be seen that the algorithm proposed in this paper was better than the MWPCA-SPE algorithm, especially for the diagnosis of B1 type faults.

5. Conclusion

Hardware redundancy is often used in engineering to enhance the fault tolerance of the system. In a redundant system with sensors, there will be problems of fault diagnosis and isolation between two sensors. In this paper, for the GG system with double pressure feedback, a novel fault diagnosis algorithm was proposed by combining the Kalman principle (knowledge-based approach), principal component analysis principle (data-driven approach), and gap metric theory (model-based approach). The simulations have shown that the method could cope well with drift failures and precision degradation failures of two sensors. This could help increase the flight safety of long-endurance aircrafts and could also provide a useful reference for other similar systems.

However, in the actual engineering system, there are some small and self-recoverable faults. The recoverability of failures and the response oscillations that fault-tolerant control may face are the next important issues to be studied.

Nomenclature

$\bar{P}$: Measured value of the GG's pressure
$\hat{P}$: Estimated value of the GG's pressure
P_g: True value of pressure inside the GG
ε_P: Individual sensor isolation thresholds
ε_H: Both sensors isolation thresholds
d: Drift rate
R: The variance when estimating pressure from N_x
θ: Valve angle
τ: Delay in estimating pressure from N_x
ε_{Hm}: Precision degradation monitoring threshold
Pe: Calculated values after improving the PCA
P_{cmd}: Pressure command
H_m: Relative health between two sensors
P_R: Output pressure of fault isolation unit
$\bar{P}_A$: The average value of the two sensors
P_B: Output pressure of PCA unit
Q_A: The variance when estimating pressure from θ
N_x: Axial overload
α: Correction coefficient
H_R: Combined health of both sensors.

Data Availability

Data used to support the findings of this study are available from the corresponding author upon request.

Conflicts of Interest

The authors declare that there is no conflict of interest regarding the publication of this paper.

Acknowledgments

This research is financially supported by the National Natural Science Foundation of China (Grant No. 61174120). I would like to show my deepest gratitude to my supervisor, Dr. Zeng Qinghua, a respectable and resourceful scholar, who has provided me with valuable guidance in every stage of the writing of this thesis.

Supplementary Materials

The Part A showed more analysis on "Consistency Index." The detailed derivation process of the equation (11) was supplemented in Part B. In addition, the simulation data on the proposed algorithm was provided in Tables S1-S5 of the Part C. *(Supplementary Materials)*

References

[1] Z. Xia, B. Chen, L. Huang, D. Wang, and M. Likun, "Research progresses in solid rocket-ramjet engine," *Aerospace Shanghai*, vol. 36, no. 6, pp. 11–18, 2019.

[2] D. L. Li, Y. Wang, J. X. Wang, C. Wang, and Y. Duan, "Recent advances in sensor fault diagnosis: a review," *Sensors and Actuators A: Physical*, vol. 309, no. 5, article 111990, 2020.

[3] M. Kordestani, M. Saif, M. E. Orchard, R. Razavi-Far, and K. Khorasani, "Failure prognosis and applications—a survey of recent literature," *IEEE Transactions on Reliability*, vol. 70, no. 2, pp. 728–748, 2021.

[4] M. Rezamand, M. Kordestani, R. Carriveau, D. S. K. Ting, M. E. Orchard, and M. Saif, "Critical wind turbine components prognostics: a comprehensive review," *IEEE Transactions on Instrumentation and Measurement*, vol. 69, no. 12, pp. 9306–9328, 2020.

[5] H. Chen, B. Jiang, S. X. Ding, and B. Huang, "Data-driven fault diagnosis for traction systems in high-speed trains: a survey, challenges, and perspectives," *IEEE Transactions on Intelligent Transportation Systems*, vol. 23, no. 3, pp. 1700–1716, 2022.

[6] H. B. Huang, T. H. Yi, and H. N. Li, "Sensor fault diagnosis for structural health monitoring based on statistical hypothesis test and missing variable approach," *Journal of Aerospace Engineering*, vol. 30, no. 2, article 4015003, 2015.

[7] H. T. Chen, B. Jiang, and N. Y. Lu, "A multi-mode incipient sensor fault detection and diagnosis method for electrical traction systems," *International Journal of Control, Automation and Systems*, vol. 16, no. 4, pp. 1783–1793, 2018.

[8] J. Y. Liu, G. N. Li, H. X. Chen, J. Wang, Y. Guo, and J. Li, "A robust online refrigerant charge fault diagnosis strategy for VRF systems based on virtual sensor technique and PCA-EWMA method," *Applied Thermal Engineering*, vol. 119, no. 3, pp. 233–243, 2017.

[9] J. Shang, D. H. Zhou, M. Y. Chen, H. Ji, and H. Zhang, "Incipient sensor fault diagnosis in multimode processes using conditionally independent Bayesian learning based recursive transformed component statistical analysis," *Journal of Process Control*, vol. 77, no. 3, pp. 7–19, 2019.

[10] Z. Long, X. F. Zhang, L. Zhang et al., "Motor fault diagnosis using attention mechanism and improved adaboost driven by multi-sensor information," *Measurement*, vol. 170, no. 11, article 108718, 2021.

[11] R. M. Souza, E. G. Nascimento, U. A. Miranda, W. J. Silva, and H. A. Lepikson, "Deep learning for diagnosis and classification of faults in industrial rotating machinery," *Computers & Industrial Engineering*, vol. 153, no. 12, article 107060, 2021.

[12] M. Mousavi, A. Chaibakhsh, A. Jamali, M. Kordestani, and M. Saif, "A new fault diagnosis approach for heavy-duty gas turbines," *IEEE/ASME Transactions on Mechatronics*, vol. 27, no. 11, article 3138834, 2021.

[13] R. Toscano and P. Lyonnet, "Diagnosis of the industrial systems by fuzzy classification," *ISA Transactions*, vol. 42, no. 5, pp. 327–335, 2003.

[14] S. U. Jan, Y. D. Lee, and I. S. Koo, "A distributed sensor-fault detection and diagnosis framework using machine learning," *Information Sciences*, vol. 547, no. 9, pp. 777–796, 2021.

[15] U. Saeed, S. U. Jan, Y. D. Lee, and I. Koo, "Fault diagnosis based on extremely randomized trees in wireless sensor networks," *Reliability Engineering and System Safe*, vol. 205, no. 10, article 107284, 2021.

[16] S. Siahpour, X. Li, and J. Lee, "Deep learning-based cross-sensor domain adaptation for fault diagnosis of electromechanical actuators," *International Journal of Dynamics and Control*, vol. 8, no. 4, pp. 1054–1062, 2020.

[17] Y. Tan, J. Zhang, H. Tian et al., "Multi-label classification for simultaneous fault diagnosis of marine machinery: a comparative study," *Ocean Engineering*, vol. 239, no. 9, article 109723, 2021.

[18] M. Rezamand, M. Kordestani, M. Orchard, R. Carriveau, D. Ting, and M. Saif, "Condition monitoring and failure prognostic of wind turbine blades," in *2021 IEEE International Conference on Systems, Man, and Cybernetics (SMC)*, pp. 1711–1718, Melbourne, Australia, 2021.

[19] Y. Fu, Z. Gao, Y. Liu, A. Zhang, and X. Yin, "Actuator and sensor fault classification for wind turbine systems based on fast Fourier transform and uncorrelated multi-linear principal component analysis techniques," *Processes*, vol. 8, no. 9, article 8091066, p. 1066, 2020.

[20] M. Kordestani, M. Rezamand, M. Orchard, R. Carriveau, D. S. K. Ting, and M. Saif, "Planetary gear faults detection in wind turbine gearbox based on a ten years historical data from three wind farms," *IFAC-PapersOnLine*, vol. 53, no. 2, pp. 10318–10323, 2020.

[21] J. Li and W. D. Qu, "Aero-engine sensor fault diagnosis based on convolutional neural network," in *2018 37th Chinese control conference (CCC)*, pp. 6049–6054, Wuhan, China, 2018.

[22] L. Chen, J. Cao, K. Wu, and Z. Zhang, "Application of generalized frequency response functions and improved convolutional neural network to fault diagnosis of heavy-duty," *Robotics and Computer-Integrated Manufacturing*, vol. 73, no. 8, article 102228, 2022.

[23] Y. G. Lei, B. Yang, X. W. Jiang, F. Jia, N. Li, and A. K. Nandi, "Applications of machine learning to machine fault diagnosis: a review and roadmap," *Mechanical Systems and Signal Processing*, vol. 138, article 106587, 2020.

[24] K. Wang, J. H. Chen, and Z. H. Song, "Data-driven sensor fault diagnosis systems for linear feedback control loops," *Journal of Process Control*, vol. 54, no. 4, pp. 152–171, 2017.

[25] W. Jiang, W. W. Hu, and C. H. Xie, "A new engine fault diagnosis method based on multi-sensor data fusion," *Applied Sciences*, vol. 280, no. 7, article 7030280, 2017.

[26] T. Chen, Z. Zhu, C. Wang, and Z. Dong, "Rapid sensor fault diagnosis for a class of nonlinear systems via deterministic

learning," *IEEE Transactions on Neural Networks and Learning Systems*, vol. 33, no. 12, article 3085533, 2021.

[27] A. H. Hassanabadi, M. Shafiee, and V. Puig, "Sensor fault diagnosis of singular delayed LPV systems with inexact parameters: an uncertain system approach," *International Journal of Systems Science*, vol. 49, no. 1, pp. 179–195, 2018.

[28] Y. Shen, L. L. Li, and Z. H. Wang, "A review of fault diagnosis and fault tolerant control techniques for spacecraft," *Journal of Astronautics*, vol. 41, no. 6, pp. 647–656, 2020.

[29] H. Q. Ji, K. K. Huang, and D. H. Zhou, "Incipient sensor fault isolation based on augmented Mahalanobis distance," *Control Engineering Practice*, vol. 86, no. 4, pp. 144–154, 2019.

[30] Y. Lin, Y. Y. Li, X. D. Yin, and Z. Dou, "Multisensor fault diagnosis modeling based on the evidence theory," *IEEE Transactions on Reliability*, vol. 67, no. 2, pp. 513–521, 2018.

[31] F. Y. Xiao, "A novel evidence theory and fuzzy preference approach-based multi-sensor data fusion technique for fault diagnosis," *Sensors*, vol. 2504, no. 17, article 17112504, 2017.

[32] K. M. Zhou, "A new framework for fault diagnosis and fault tolerant control," *Acta Auto-Matica Sinica*, vol. 47, no. 5, pp. 1035–1042, 2021.

[33] Y. Wang, P. He, P. Shi, and H. Zhang, "Fault detection for systems with model uncertainty and disturbance via coprime factorization and gap metric," *IEEE Transactions on Cybernetics*, vol. 52, no. 8, article 33566789, 2021.

[34] H. Jin, Z. Zuo, Y. Wang, L. Cui, and L. Li, "An integrated model-based and data-driven gap metric method for fault detection and isolation," *IEEE Transactions on Cybernetics*, vol. 52, no. 12, article 34236975, 2021.

[35] Y. Xin, H. X. Wu, and X. L. Wang, "A review of spacecraft fault diagnosis and fault tolerant control technology," *Journal of Astronautics*, vol. 24, no. 3, pp. 221–226, 2003.

[36] D. H. Zhou, Y. Liu, and X. He, "Review on fault diagnosis techniques for closed-loop systems," *Acta Automatica Sinica*, vol. 39, no. 11, pp. 1933–1943, 2013.

[37] X. Q. He, *Research of Principal Component Analysis and Its Application in Data Reconstruction of Fault Sensor, [Ph.D. Thesis]*, Northeastern University, Shenyang, China, 2010.

[38] A. Wang, Q. H. Zeng, L. K. Ma, and H. Wang, "Virtual free-volume revised method and adaptive control for solid ducted rockets," *Journal of Aerospace Engineering*, vol. 34, no. 5, article 04021053, 2021.

[39] J. E. Jackson and G. S. Mudholkar, "Control procedures for residuals associated with principal component analysis," *Technometrics*, vol. 21, no. 3, pp. 341–349, 1979.